

# Flashing flexodomains and electroconvection rolls in a nematic liquid crystal

Péter Salamon<sup>1</sup>, Nándor Éber<sup>1</sup>, Alexei Krekhov<sup>2</sup> and Ágnes Buka<sup>1</sup>

<sup>1</sup> *Institute for Solid State Physics and Optics, Wigner Research Centre for Physics, Hungarian Academy of Sciences, H-1525 Budapest, P.O.B.49, Hungary and*

<sup>2</sup> *Institute of Physics, University of Bayreuth, D-95440 Bayreuth, Germany*

(Dated: March 3, 2022)

Pattern forming instabilities induced by ultralow frequency sinusoidal voltages were studied in a rod-like nematic liquid crystal by microscopic observations and simultaneous electric current measurements. Two pattern morphologies, electroconvection (EC) and flexodomains (FD), were distinguished; both appearing as time separated flashes within each half period of driving. A correlation was found between the time instants of the EC flashes and that of the nonlinear current response. The voltage dependence of the pattern contrast  $C(U)$  for EC has a different character than that for the FD. The flattening of  $C(U)$  at reducing the frequency was described in terms of an imperfect bifurcation model. Analysing the threshold characteristics of FD the temperature dependence of the difference  $|e_1 - e_3|$  of the flexoelectric coefficients were also determined by considering elastic anisotropy.

PACS numbers: 61.30.Gd, 47.54.-r

## I. INTRODUCTION

Nematic liquid crystals are the simplest paradigm for anisotropic fluids; i.e. liquids with a preferred direction of the orientation of molecules with anisotropic shape which is described by the director field  $\mathbf{n}$ . The anisotropy of their dielectric properties allows controlling the director by electric fields. The (usually homogeneous) reorientation of the director by a properly applied voltage changes the direction of the optical axis and hence the light transmittance of the sample; this forms the physical background of the liquid crystal displays, [1] used widespread in common electronic devices.

Applying an electric voltage to a nematic liquid crystal layer can, however, often result in the appearance of spatio-temporal, periodic or disordered structures too. The conditions of their occurrence, the pattern morphologies and their onset characteristics have been extensively studied since decades, both experimentally and theoretically [1–14].

In the mostly studied planar configuration, where the director is initially oriented parallel to the confining plates, one of the electric field induced patterns corresponds to spatially periodic, equilibrium director deformations (seen as stripes parallel to the director in a polarizing microscope), occurring due to a flexoelectric free energy gain of the deformed state; therefore they have been coined *flexoelectric domains* (FDs) [2]. FDs have so far been detected in a few nematic compounds only and they are observable at DC (or very low frequency AC) driving only.

A more frequent, but also more complex pattern forming phenomenon is the electroconvection (EC) where the director distortions are accompanied by space charge separation and hence by material flow; thus having a dissipative character. It could be observed in many nematics, some of which possess substantially different material properties [3, 4]. EC patterns could be induced in a wide

frequency range of the applied voltage (ranging from DC up to several hundreds kHz AC); the resulting convection rolls are seen in a polarizing microscope as stripes whose direction may be normal to, oblique or parallel with the director. Up to now studies were mostly focussed on the class of nematics with negative dielectric and positive conductivity anisotropies and on driving frequencies  $f$  within the range of 10 Hz to 10 kHz. In this  $f$  range evolution of the pattern requires numerous driving periods after voltage application. For such conditions the variation of pattern morphologies (conductive and dielectric regimes, oblique and normal rolls) upon the amplitude and frequency of the applied voltage have been explored in detail and the mechanism as an electrohydrodynamic instability has been well understood. A quantitative theoretical description of the pattern threshold, the critical wave vector and some secondary transitions (e.g. abnormal rolls) could be given combining nematodynamics with electrodynamics under the simplifying assumption of Ohmic conductivity – now called as the standard model of EC [5] – or via its extensions by flexoelectricity [6] or by ionic diffusion/recombination [7].

Recently interest has arisen to study the behaviour in another, subhertz frequency range, where the pattern growth/decay times are (much) shorter than the driving period, using compounds which may exhibit both EC and FD patterns. It has been proven experimentally that at such ultralow frequencies both for the dielectric [8] and the conductive [9] EC regimes, as well as for the FD [8, 9] the patterns are flashing, i.e. they exist only in a small part of the driving period. It has been found that there is an  $f$  range ( $\sim 1 - 100$  mHz) where both EC and FD patterns can exist in each driving half period in the form of successive (time shifted) flashes. Theoretical calculations based on the standard model of EC extended with flexoelectricity [6] (which is able to describe FDs too [10]) have justified that flashing patterns are indeed the solutions of the nemato-electrohydrodynamic equa-

tions at ultralow  $f$ . The calculated position of the FD flashes within the driving half period showed quantitative matches with the experiments, while for the position of the EC flashes the frequency dependence was only qualitatively reproduced by the calculations, as the EC flashes come earlier within the period than expected [9].

In this paper we present further experimental results on the ultralow  $f$  behaviour, however, in a different system than those reported before. The paper is organized as follows. Section II introduces our compound and the experimental method. The new findings are grouped around three subtopics: Section III A reports on the temporal evolution of the patterns within the period; Section III B deals with the frequency dependence of the threshold characteristics and Section III C provides data on the temperature dependence of various material parameters. Finally the paper is concluded in Section IV with a summary and some closing remarks.

## II. EXPERIMENTAL

Our measurements have been performed on the nematic liquid crystal 4-n-octyloxyphenyl 4-n-methoxybenzoate (10O8)<sup>1</sup> that shows only a nematic mesophase. The chemical structure of 10O8 is shown in Fig. 1.

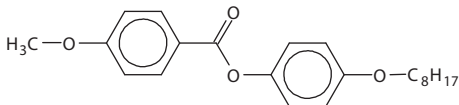


FIG. 1. The chemical structure of the rod-like nematic molecule 4-n-octyloxyphenyl 4-n-methoxybenzoate (10O8).

In heating it melts to nematic from the crystalline phase at 63.5 °C, while the clearing point ( $T_{NI}$ ) equals to 76.7 °C. The nematic phase can be supercooled down to 53°C. The material parameters of 10O8, such as the dielectric anisotropy ( $\varepsilon_a = \varepsilon_{\parallel} - \varepsilon_{\perp}$ ), the optical anisotropy ( $n_a = n_{\parallel} - n_{\perp}$ ), the anisotropy of the diamagnetic susceptibility ( $\chi_a = \chi_{\parallel} - \chi_{\perp}$ ), and the bulk elastic constants ( $K_{11}, K_{22}, K_{33}$ ) were determined as the function of temperature using a method based on magnetic and electric Freedericksz-transitions [15]. Here  $\varepsilon$  and  $n$  denote the dielectric permittivity and the refractive index, respectively; the subscripts  $\parallel$  and  $\perp$  correspond to measurement directions parallel with and perpendicular to the director.

The compound was investigated in commercial sandwich cells (E.H.C. Co.) with ITO electrodes coated with

rubbed polyimide layers for planar alignment. The electrode area was 1 cm<sup>2</sup>. The thickness of the empty cells ( $d = 10.4 - 10.8 \mu\text{m}$ ) was measured by an Ocean Optics spectrophotometer. During the measurements the temperature of the sample was kept constant within 0.01 °C in an Instec HSi heat stage controlled with an mK-1 board. The sample was driven by a sinusoidal voltage  $\tilde{U}(t)$  of an Agilent 33120A function generator via a high-voltage amplifier:  $\tilde{U}(t) = \sqrt{2}U \sin(2\pi ft)$ .

The electric field induced patterns were observed by a Leica DM RX polarizing microscope in transmission mode with white light illumination using the shadow-graph technique [17] (the polarizer was removed, while the analyser was set to be parallel with the rubbing direction). The imaging system was equipped with an EoSens MC1362 high speed camera interfaced by an Inspecta-5 frame grabber. After waiting one or two periods of the driving signal following the application of the voltage to the sample (or waiting 5 seconds at frequencies higher than 0.2 Hz), a sequence of 1000 images was recorded. The acquisition of the first image was triggered by the zero crossing (from negative to positive) of the applied voltage.

In addition to the optical observations the electric current through the cell was monitored by measuring the voltage drop on a relatively small, known resistance connected in series with the sample. Simultaneously the driving waveform was also recorded by a TiePie Handyscope HS3 oscilloscope. The data acquisition and processing system was fully automated.

## III. RESULTS AND DISCUSSION

### A. Flashing contrast and current

Applying a low frequency (e.g.  $f = 50$  mHz) sinusoidal voltage to the cell, patterns appear above a threshold voltage in a narrow time window in each half period of driving. Two distinct pattern morphologies were found with different thresholds, similarly to previous observations on other nematics [9]. Representative snapshots of the patterns and their 2-dimensional (2-d) Fourier transforms (the spectral intensities) are presented in Fig. 2. The two morphologies can be attributed to oblique conductive EC rolls (a zig-zag pattern, Fig. 2a) and to flexodomains (Fig. 2b); the latter appear as stripes parallel to the initial director alignment.

For a quantitative analysis of the pattern evolution it is necessary to provide a proper definition for the pattern contrast, which has a minimum (ideally zero) in the homogeneous state and increases as the pattern emerges.

A common procedure is to perform a 2-d Fourier transformation of the images in order to find the critical wave vector  $\mathbf{q}_c = (q_x, q_y)$  of the pattern (where the Fourier amplitudes have maxima) and to define the contrast  $C_q$  as the sum of the spectral intensities in a region around  $\mathbf{q}_c$ . It is clear from Fig. 2 that the two pattern types observed

<sup>1</sup> Two abbreviation styles are known in the literature for the members of the 4-n-alkyloxyphenyl 4-n-alkyloxybenzoate homologous series. Here we have adopted the one used by Nair et al. [16] According to the alternative style by Kochowska et al.[13] the same compound could also be abbreviated as 1/8.

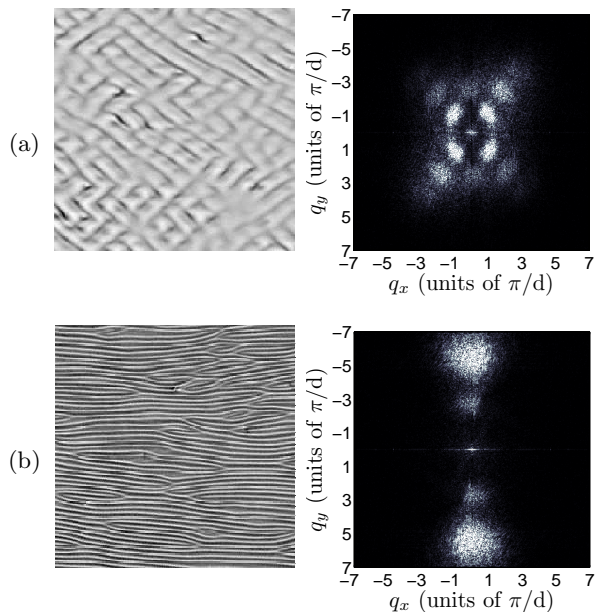


FIG. 2. Snapshot images and their 2-d Fourier transforms (a) for electroconvection and (b) for flexodomains at  $f = 50$  mHz and  $U = 19$  V. The images cover  $200 \mu\text{m} \times 200 \mu\text{m}$  area. The initial director orientation lies horizontally.

in 1008 (EC and FD) are characterized by different  $\mathbf{q}_c$  vectors, i.e. they are well separated in the Fourier space. Therefore this contrast definition allows distinguishing them not only from the initial homogeneous state, but also between each other.

Alternatively, a mean square deviation of the image intensities,  $C_s = \langle (\Phi - \langle \Phi \rangle)^2 \rangle$ , may also serve as a measure of the contrast. Here  $\Phi$  is the intensity of an individual pixel and  $\langle \rangle$  denotes averaging over the whole image. This definition is simpler, though it has the disadvantage of not being able to distinguish various pattern morphologies. Actually  $C_s$  would coincide with  $C_q$  if the summation of the spectral intensities were extended over the whole Fourier space.

Figure 3 exhibits and compares the time dependence of contrast within a driving period for both definitions given above, measured in a  $d = 10.4 \mu\text{m}$  thick cell at  $T - T_{NI} = 21.7$  °C driven by an  $f = 22$  mHz,  $U = 18$  V voltage. Figure 3a shows  $C_q$  obtained by the Fourier method for the EC (solid line) and the FD (dashed line) patterns. Both curves exhibit a single peak in each half period, but at different time intervals; hence these two pattern types are well separated not only in the Fourier space, but in time as well. In Fig. 3b the contrast  $C_s$  calculated by the square deviation is plotted. This curve has two, well separated peaks per half period (looks similar to the superposition of the two curves in Fig. 3a); thus can also be used to detect the appearance of both pattern types. Therefore, for simplicity, in the following we will use  $C_s$  as the measure of the contrast of the patterns.

Figure 3c depicts the time dependence of the electrical

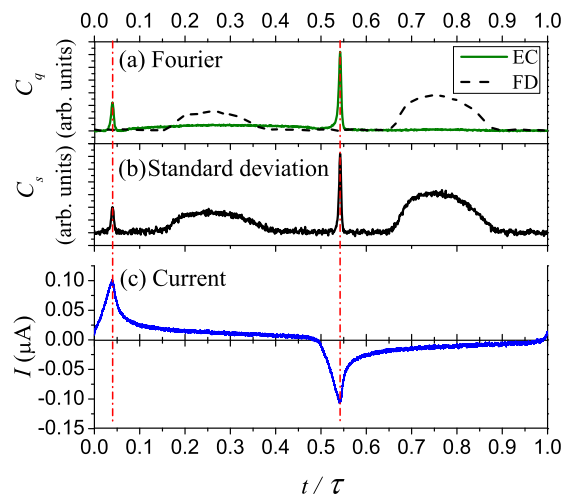


FIG. 3. (Color online) The time dependence within a driving period (a) for the contrast  $C_q$  obtained by Fourier technique; (b) for the contrast  $C_s$  calculated from the square deviation; and (c) for the electrical current  $I$  through the liquid crystal.  $t = 0$  corresponds to the zero crossing (from positive to negative) of the applied voltage. The dashed-dotted lines show that the peaks of EC and of the current coincide.

current which was measured simultaneously with image acquisition. At this  $f$  and  $U$  the current is highly nonlinear; it can be characterized by sharp peaks rather than by a harmonic response. It can be deduced from the figure that, surprisingly, the location of the maxima of the current peaks coincide precisely with the contrast peaks corresponding to the EC flashes (see the dash-dotted vertical lines in Fig. 3). Numerous different voltages, frequencies and temperatures were tested. Though at various conditions the time instant of the EC flash may change [9], it still equals to that of the current peak; thus we can conclude that this is not an accidental coincidence. We suggest that the current spikes trigger the emergence of the EC pattern. Therefore it appears earlier within the half period (a phase-locking behaviour) than expected otherwise.

We note that the spiky behaviour of the current is not a consequence of the appearance of the EC pattern. Current spikes have been detected at low voltages (much below any pattern threshold) where no patterns are observable and also in the isotropic phase. We think that the nonlinear current behaviour is due to ionic effects and to the presence of insulating polyimide orienting layers on the electrode surfaces of the cell. The presence of (relatively low) concentration of ionic impurities in the nematic makes it to behave as a weak electrolyte. In the studied ultralow frequency range the current due to the linear impedance of the cell (i.e. the capacitive and the ohmic components) is at least an order of magnitude smaller than the transient currents due to building or destroying the Debye screening layers near the electrodes; the latter occurs at each polarity reversal of the voltage.

In order to describe the behaviour of weak electrolytes in electric fields several models were developed, differing in their sets of assumptions [18–26]; i.e. they take into consideration different subsets of the possible effects listed below: generation and recombination of ions; different mobilities, diffusion coefficients and charges of ionic species; surface adsorption; charge injection; chemical reactions; voltage attenuation due to the orienting layers; etc. Due to the complexity of the models they mostly focused on the linear response and calculated the low frequency complex impedance which could be compared to low  $f$  dielectric spectroscopy data.

Recently theoretical calculations of the nonlinear current characteristics in response to a low frequency sinusoidal voltage driving were also reported [18, 19], yielding curves similar to those shown in Fig. 3c, however, without comparison with experiments. This gives the hope that after measurements or intelligent guesses of the unknown material parameters of the model the measured current response can be reproduced; it is remaining a task for the future.

The nematic being a weak electrolyte has consequences on the pattern formation processes. It was shown that the weak electrolyte model (WEM) of EC [7], which considers ionic dissociation and recombination, can account for the travelling of EC roll patterns found occasionally at frequencies above a few tens Hz. This model has not yet been analysed for low driving frequencies; due to its high complexity it remains a challenge for the future to decide whether it is able to describe the phase locking of EC flashes to current spikes.

## B. Threshold characteristics

Flexodomains and electroconvection both are threshold phenomena; i.e. the patterns with a critical wavenumber  $q_c = |\mathbf{q}_c|$  occur above a threshold voltage  $U_c$ . Determination of  $U_c$  and  $q_c$  is therefore the primary task at pattern characterization. At high frequencies ( $f > 10$  Hz) for  $U > U_c$  patterns usually develop within seconds; therefore thresholds can easily be estimated by increasing  $U$  as the voltage at which the pattern becomes perceptible by eyes in the microscope. This simple technique practically does not work at our ultralow frequency driving, since the driving period is quite long and in addition the patterns appear as flashes, which means they can be observed only in a short time window.

In order to determine  $U_c$  precisely one has to follow quantitatively the emergence of patterns from the homogeneous state; i.e. to record and then analyse the contrast-voltage curves. As the contrast varies within the driving period (as shown in Fig. 3b), the maximum  $C_m$  of the contrast  $C_s$  in the FD (or EC) peak can be regarded as a measure to what extent the FD (or EC) pattern has been developed at a given applied voltage.

In an ideal case (perfect bifurcation) the contrast  $C_m$  should be zero at voltages below the threshold. Exper-

imentally a nonzero background contrast  $C_b$  is always found even in the homogeneous state at no applied voltage ( $C_b = C_s(U = 0)$ ). This background contrast comes from various sources: the electronic noise of the camera, the thermal fluctuation of the director in a planar nematic, imperfections of the orientation or inhomogeneity of the illumination. This background was automatically subtracted from each data point; thus it will not be indicated in the forthcoming figures.

As the voltage is increased above  $U_c$ , the initial planar director orientation  $\mathbf{n}_0 = (1, 0, 0)$  becomes unstable and a spatially periodic director distortion  $\delta\mathbf{n} = \mathbf{n}_{lin} A \exp[i(q_x x + q_y y)]$  appears. Here  $\mathbf{n}_{lin} = (0, n_y, n_z)$  is a linear eigenvector,  $A \propto \sqrt{U^2 - U_c^2}$  characterize the amplitude of the distortion, and  $\mathbf{q}_c = (q_x, q_y)$  is the wavevector of the pattern. The spatially periodic director distortion results in a shadowgraph image whose intensity modulation  $I_s$  depends on the amplitude of the vertical distortion  $An_z$ . For small distortion amplitudes (not too far from threshold) the intensity modulation in the leading order is given[27] by  $I_s = c_a A + c_p A^2$  with the first order amplitude term and the second order phase term. For EC patterns (normal rolls with  $\mathbf{q}_c = (q_x, 0)$ ) the linear term is dominating and  $I_s \propto A$ . In case of FD, where  $\mathbf{q}_c = (0, q_y)$ , the relevant contribution to the shadowgraph intensity is of the second order: [28]  $I_s \propto A^2$ . The contrast of the shadowgraph image defined as the mean square deviation of the image intensities is then  $C_s \propto I_s^2$ . Thus the maximum of the contrast within the driving period is expected to be  $C_{mEC} \propto (U^2 - U_{cEC}^2)$  for an EC pattern and  $C_{mFD} \propto (U^2 - U_{cFD}^2)^2$  for the FD [8]. In the vicinity of the threshold  $(U^2 - U_{cFD}^2) \approx 2U_c(U - U_c)$ ; therefore  $C_{mEC}$  as well as  $\sqrt{C_{mFD}}$  should grow linearly with the voltage.

Figure 4 shows the measured  $\sqrt{C_{mFD}}(U)$  curves for a few frequencies. It is seen that the linear relation near the threshold is obeyed quite well; though the transition is smeared a little (due to imperfections and/or the occurrence of subcritical fluctuations). Therefore the threshold voltage  $U_{cFD}$  is actually determined by a linear extrapolation, as the intersection of the horizontal axis with the line fitted onto the linear section of the  $C_m(U)$  curve slightly above the suspected threshold. This procedure is going to be referred as method A.

The voltage dependence of  $C_{mEC}$  for EC is shown in Fig. 5 for several driving frequencies. It is clearly seen that the frequency affects not only the threshold voltages, but also the character (the shape) of the  $C_{mEC}(U)$  curves. Evidently the linear relation holds only at high frequencies; there the thresholds  $U_{cECA}$  can be determined by extrapolation (method A).

Below 1 Hz, however, there is no sharp increase of the contrast; the  $C_m(U)$  curves show rather a slow gradual increase, while the contrast levels and thus the visibility of the patterns vary in the same range as at high frequencies. The determination of thresholds is then not so straightforward. In lack of a well defined linear part of the contrast curve, method A becomes unreliable; the

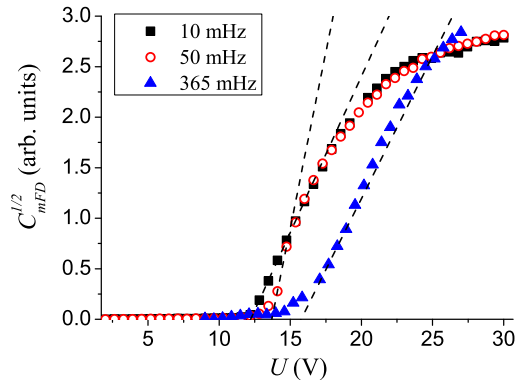


FIG. 4. (Color online) The voltage (rms) dependence of the square root of the FD contrast peaks for different frequencies (symbols). The dashed lines indicate the linear extrapolation.

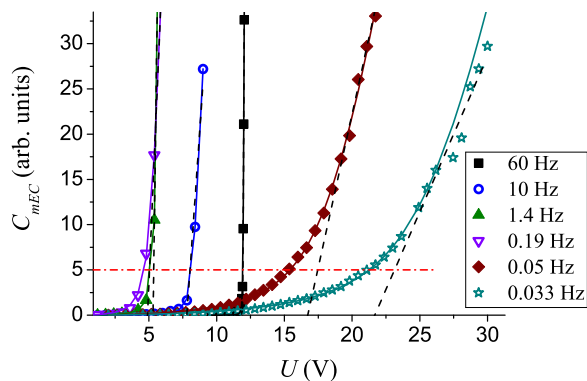


FIG. 5. (Color online) The voltage (rms) dependence of the contrast peaks  $C_m$  of EC for different frequencies (symbols). Solid lines are fits with the imperfect bifurcation model, the dashed lines indicate the linear extrapolation.

choice of points used for the extrapolation (the dashed lines in Fig. 5) is to some extent arbitrary.

An alternative way (method B) is to select (arbitrarily) a critical contrast value  $C_0$  (the dash-dotted line in Fig. 5) where the EC pattern is visible by eye. The voltage  $U_{cECB}$ , where  $C_{mEC}(U_{cECB}) = C_0$ , can be regarded as another estimate of the threshold. In case of forward bifurcations, which the standard EC pattern formation is an example for, the contrast increases continuously from zero. Therefore  $U_{cECB}$  slightly overestimates the threshold.

The change in the shape of the  $C_{mEC}(U)$  curves may be interpreted so that the nearly perfect bifurcation (at high  $f$ ) becomes imperfect at lower  $f$ . For an imperfect bifurcation the amplitude of the director distortion  $A$  satisfies the equation

$$\varepsilon A - gA^3 + \delta = 0. \quad (1)$$

Here  $\varepsilon = U^2/U_{cEC}^2 - 1$ ,  $U$  is the rms applied voltage,  $U_{cEC}$  is the threshold voltage,  $g > 0$  characterizes the saturation of the amplitude and  $\delta \geq 0$  is the measure for the imperfection ( $\delta = 0$  corresponds to the perfect forward bifurcation). For  $g > 0$  and  $\delta > 0$  only one of the three solutions of Eq. (1) is stable in the whole range of  $\varepsilon > -1$  and thus relevant; it reads as

$$A = \left(\frac{\delta}{2g}\right)^{1/3} F(\tilde{\varepsilon}),$$

$$F(\tilde{\varepsilon}) = \left(\frac{\tilde{\varepsilon}}{\hat{f}(\tilde{\varepsilon})} + \hat{f}(\tilde{\varepsilon})\right) \text{ for } \tilde{\varepsilon} \leq 1, \quad (2)$$

$$F(\tilde{\varepsilon}) = 2\sqrt{\tilde{\varepsilon}} \cos\left(\frac{1}{3} \arctan(\sqrt{\tilde{\varepsilon}^3 - 1})\right) \text{ for } \tilde{\varepsilon} > 1,$$

$$\tilde{\varepsilon} = \frac{2}{3} \frac{\varepsilon}{(2g\delta^2)^{1/3}}, \quad \hat{f}(\tilde{\varepsilon}) = (1 + \sqrt{1 - \tilde{\varepsilon}^3})^{1/3}.$$

As mentioned above, the maximum contrast  $C_{mEC}$  of the EC patterns observed using the shadowgraph technique is proportional to  $A^2$ . In Fig. 6 the dependence of  $A^2$  on the applied voltage  $U$  is shown for different values of the imperfection parameter  $\delta$  at fixed values of  $U_{cEC}$  and  $g$ . It demonstrates that the shape of the curve changes substantially if the imperfection ( $\delta$ ) increases.

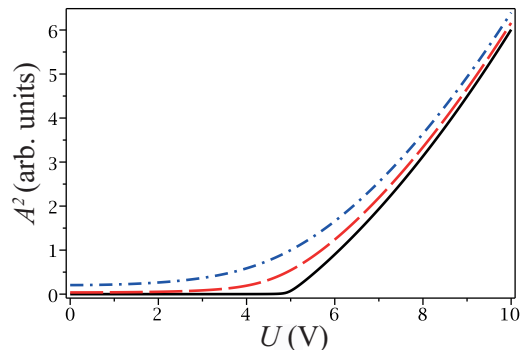


FIG. 6. (Color online) Square of the pattern amplitude  $A^2$  as a function of the applied voltage  $U$  for  $\delta = 0.01$  (solid line),  $\delta = 0.2$  (dashed line), and  $\delta = 0.5$  (dot-dashed line).  $U_{cEC} = 5$ ,  $g = 0.5$ .

For a precise quantitative analysis we can use the same background subtraction here, just as was done with the experimental data; therefore the contrast depicted in Fig. 5 will be related to the amplitude as:

$$C_{mEC} = C_{max} - C_b = \alpha[A^2(U) - A^2(U = 0)], \quad (3)$$

where  $C_{max}$  is the maximum contrast of the pattern,  $C_b$  is the background contrast at  $U = 0$ , and  $\alpha > 0$  is a scaling factor. Combining Eqs. (2) and (3) one can fit the experimental  $C_{mEC}(U)$  curves by this phenomenological model for imperfect bifurcation using four parameters:  $\alpha$ ,  $g$ ,  $\delta$  and  $U_{cEC}$  (method C).

The actual value of the scaling parameter  $\alpha$  is determined by the optical set-up and the optical properties. As  $q_c$  of the EC pattern depends weakly on  $f$ , we can assume that  $\alpha$  is frequency independent. Its value could be obtained from the fit at  $f = 60$  Hz, leaving only three free parameters for the fits at lower frequencies.

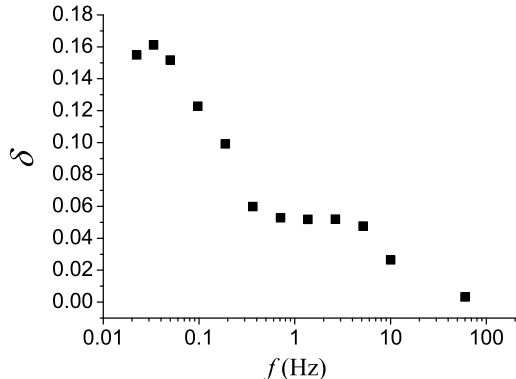


FIG. 7. Frequency dependence of the imperfection parameter  $\delta$ .

The results of the fit procedure are shown by solid lines in Fig. 5. The match with the experimental data are quite convincing. The frequency dependence of the imperfection parameter  $\delta$  is plotted in Fig. 7. It clearly shows – what we have already expected from the experimental data in Fig. 5 – that the imperfection grows at lower frequencies. Several reasons could be responsible for the increase of the apparent imperfection.

In planar samples aligned by rubbed polyimide layers a small director pretilt at the confining plates is practically unavoidable. Such pretilt is known to yield imperfect bifurcation (i.e. lack of a sharp threshold) in the case of splay Freedericksz-transition. The effect of a tilted alignment on the EC characteristics has theoretically been studied only for high frequencies [29]; the pretilt modified  $U_c$ , but did not affect the sharpness of the threshold, which is in agreement with our observations (Fig. 5) at high  $f$ .

Decreasing the frequency of the applied ac voltage well below the inverse director relaxation time may, however, alter the situation as one enters the regime of quasistatic director response. Here a small pretilt may enhance the director deformations and correspondingly the contrast of the pattern can develop already at lower voltage amplitudes compared to the high frequency case. Unfortunately a detailed theoretical analysis of this regime in the presence of pretilt is not yet available.

The nonlinear electric current characteristics presented in Sec. III A may provide another reason for the apparent softening of the ultra-low  $f$  EC thresholds. The coincidence of the electric current peaks and the EC flashes clearly shows the strong correlation between pattern formation and ionic phenomena: the massive ionic flow helps the electro-hydrodynamical instability to emerge.

The spatial distribution of the current is not necessarily uniform, mainly due to surface inhomogeneities (which may originate e. g. from crystallization of the compound) or small variations in the cell thickness and/or pretilt. The current inhomogeneities may locally reduce the threshold of EC. In fact this effect has been observed: the EC pattern first appears in germs and extends gradually to larger area by increasing the voltage. The location of these germs can be identified even in the well developed pattern as small spots/patches of higher contrast (a few such spots can be seen in Fig. 2a). The contrast  $C_{mEC}(U)$  of the pattern plotted in Fig. 5 is calculated over the whole image; thus a continuous increase of the area filled with pattern leads to a continuous increase of  $C_{mEC}(U)$ . Consequently a locally sharp transition yields a softened, gradual contrast variation. While ionic effects are mostly negligible at high frequencies (linear current response), they become crucial at ultralow frequencies (spiky current response), which may explain the increase of the imperfection parameter for  $f \rightarrow 0$ .

We note that the formation of flexodomains is not affected by the electric current spikes as they occur in different time windows. Therefore the above scenario of germ-induced pattern evolution does not apply to FD; i.e. the onset of FD remains sharp over the full frequency range of its existence, as shown in Fig. 12.

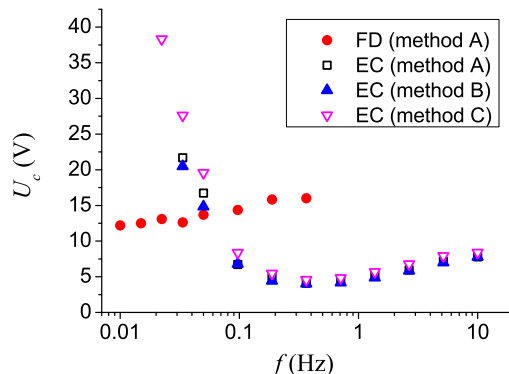


FIG. 8. (Color online) The frequency dependence of threshold voltages (rms) of EC and FD determined by various methods.

The frequency dependence of the threshold voltages of both patterns can be seen in Fig. 8. It depicts the  $U_{cEC}$  values determined by all three methods introduced above. The data by methods A (extrapolation) and B (comparison) almost coincide, while the thresholds obtained from fitting to the imperfect bifurcation model are significantly larger at lower frequencies. This is not surprising since methods A and B intrinsically assume that no deformation exists below a threshold, while an imperfect bifurcation actually means a thresholdless deformation with  $U_c$  being a parameter only.

Otherwise the  $U_{cEC}(f)$  curve exhibits the expected behaviour. The reduction of the threshold at lowering  $f$  in

the  $0.5 < f < 10$  Hz range corresponds to the theoretical predictions and matches the behaviour of other nematics [30]. The increase of  $U_{cEC}$  toward ultralow frequencies is attributed to the internal attenuation due to the insulating polyimide alignment layers on the electrodes [9]. The frequency dependence of  $U_{cFD}$  seems to be significantly weaker than that of  $U_{cEC}$  in the same  $f$  range. Taking into account the internal attenuation, the actual FD threshold voltage (on the liquid crystal layer) grows much stronger with  $f$  than the apparent threshold plotted in the figure (the voltage applied to the cell), which is in agreement with the theoretical predictions [10].

Figure 8 clearly shows that the two distinct patterns, EC and FDs, coexist in a relatively wide ( $0.02 \text{ Hz} < f < 0.4 \text{ Hz}$ ) range, even though their threshold voltages are quite different. This is possible, because they remain separated in time until the half period of driving voltage is large enough for both patterns to emerge and decay; thus they can build up from the same almost homogenous initial state. For  $f > 0.4 \text{ Hz}$ , however, this does not hold any more. In that range, besides the shorter period time,  $U_{cEC}$  is much lower than  $U_{cFD}$ . Thus the EC contrast spikes become much broader and the EC pattern does not decay fully before FD should emerge. Under such condition the FD pattern (which has a lower contrast than EC) cannot be recognized any more.

As the frequency is reduced, at around  $0.05 - 0.07 \text{ Hz}$  there is an intersection of the two threshold curves ( $U_{cFD}$  and  $U_{cEC}$ ). At  $f$  below this intersection the threshold of FDs is lower than that of EC; thus upon increasing the voltage FD is the first instability, EC sets on at a higher voltage. This is in accordance with the finding that when applying a pure DC voltage, no EC pattern, only FDs can be detected.

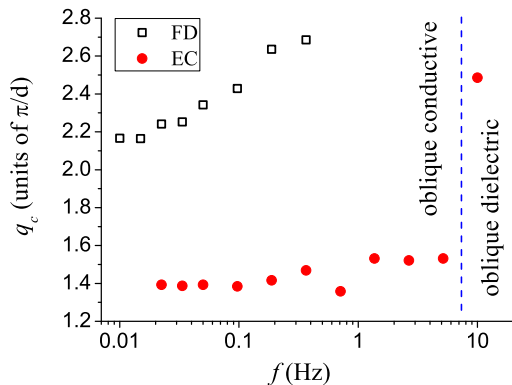


FIG. 9. (Color online) The frequency dependence of the threshold wave numbers for EC and FD.

Characterization of the threshold behaviour is incomplete without addressing the frequency dependence of the critical wave number  $q_c = |\mathbf{q}_c|$ . Figure 9 exhibits the relevant curves both for EC ( $q_{cEC}$ ) and FD ( $q_{cFD}$ ). The values were determined using the 2-d fast Fourier transformation (FFT) of images taken slightly above the thresh-

old, at  $U = 1.05U_c$ , in order to have sufficient contrast for the evaluation. Note that for the oblique EC rolls  $q_{cEC} = \sqrt{q_x^2 + q_y^2}$ , while FDs are parallel to the initial director, so  $q_{cFD} \approx q_y$ . The wave numbers increase for both patterns with the frequency. In the case of FD there is a moderate  $f$  dependence even at ultralow frequencies. For EC, the change of  $q_{cEC}$  seems to be very small until 5 Hz. Between 5 and 10 Hz, however, the wave number increases suddenly, which is attributed to the transition between oblique conductive and oblique dielectric EC. To our knowledge no such transition was reported before in the literature. We note that the obliqueness angle decreases with the frequency, the Lifshitz-point is reached in the dielectric regime at  $f_L \approx 80 \text{ Hz}$ .

### C. Temperature dependence of the flexoelectric coefficients

Though several experimental methods have been proposed to measure the flexoelectric coefficients, measurements usually cannot be done without serious compromises [14]. Analysis of the threshold parameters ( $q_{cFD}$ ,  $U_{cFD}$ ) of the flexoelectric instability is one of the possible methods. Its drawback is that only a few compounds exhibit this effect, because: 1) the material needs to have a quite low dielectric anisotropy ( $|\varepsilon_a| \ll 1$ ), 2) the concentration of its ionic impurities should be sufficiently low in order to avoid large screening effects, 3) other phenomena (e.g. EC or Fredericksz-transition) should not influence the homogenous planar initial state below the threshold of FD.

The threshold characteristics for dc driving voltage have long ago been calculated analytically [2] using the one-elastic-constant approximation ( $K_{11} = K_{22} = K$ ):

$$\tilde{U}_{cFD} = \frac{2\pi K}{|e_1 - e_3|(1 + \mu)}, \quad (4)$$

$$\tilde{q}_{cFD} = \frac{\pi}{d} \sqrt{\frac{1 - \mu}{1 + \mu}}, \quad (5)$$

where  $e_1$  and  $e_3$  are the splay and bend flexoelectric coefficients, respectively, and

$$\mu = (\varepsilon_0 \varepsilon_a K) / |e_1 - e_3|^2. \quad (6)$$

According to Eq. (5) the flexodomains can only exist for the material parameter combination  $|\mu| < 1$ . This leads to the requirement  $|\varepsilon_a| < |e_1 - e_3|^2 / (\varepsilon_0 K)$  that should be valid for materials showing FDs. Combining Eqs. (5) and (6) yields:

$$|e_1 - e_3| = \sqrt{\varepsilon_0 \varepsilon_a K \frac{1 + q_{cFD}^2}{1 - q_{cFD}^2}}. \quad (7)$$

For 10O8 both  $q_{cFD}$  and  $U_{cFD}$  were measured as the function of temperature using 10 mHz ac sine voltage. We assumed that 10 mHz is low frequency enough to be considered as a quasistatic case, hence we have fitted the results with a static model. Therefore  $U_{cFD}$  here is presented in voltage amplitude values instead of rms, since FD appears when the driving voltage reaches its maxima. Therefore  $U_{cFD}$  in Fig. 10 is presented in voltage amplitudes instead of rms values.

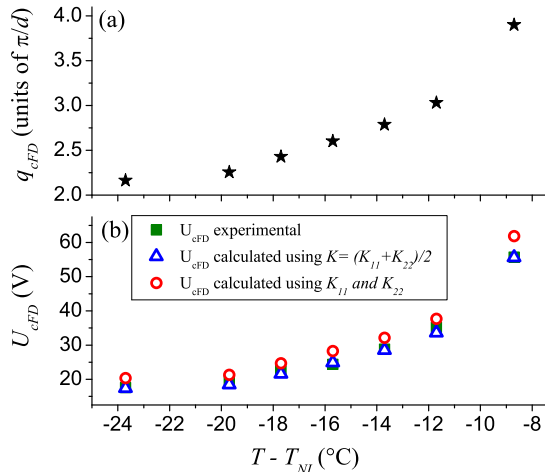


FIG. 10. (Color online) The temperature dependence of (a) the wave number  $q_{cFD}$  and (b) the voltage  $U_{cFD}$  (amplitude) at the onset of flexodomains.

Both  $q_{cFD}$  and  $U_{cFD}$  increase strongly toward higher temperatures. Above  $T - T_{NI} = -8$  °C we could not detect flexodomains up to the voltage of 135 V.

In order to determine  $|e_1 - e_3|$  we have measured some material parameters of 10O8 using methods based on electric and magnetic Fredericksz-transitions. The temperature dependence of  $\varepsilon_a$  and of the diamagnetic susceptibility anisotropy ( $\chi_a$ ) is shown in Fig. 11a.  $\varepsilon_a$  is negative and relatively small, as it was expected. Therefore in our planar sandwich cell geometry the dielectric interaction stabilizes the planar structure; no electric field induced Fredericksz-transition occurs. The values and the thermal behaviour of  $\chi_a$  are in the regular range of those in rod-like nematics. This also holds for the elastic constants  $K_{11}$ ,  $K_{22}$ , and  $K_{33}$ , which are plotted in Fig. 11b. We note that  $K_{33}$  is shown only for the sake of completeness; we do not use it further on.

The temperature dependence of  $|e_1 - e_3|$ , presented in Fig. 12, was calculated from the measured data by two different techniques. The first method (square symbols) was based on the analytical formula, Eq. (7), of the one-elastic-constant approximation, taking  $K = (K_{11} + K_{22})/2$ . The second technique (triangle symbols) utilized the recent theory [10] of flexoelectric domains that takes into account the anisotropic elasticity ( $K_{11} \neq K_{22}$ ), calculating  $|e_1 - e_3|$  numerically. As seen in Fig. 12, the second method provided values about 7%

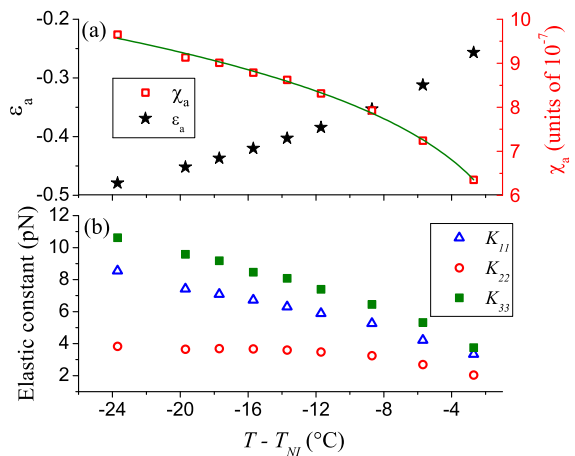


FIG. 11. (Color online) The temperature dependence of (a) the dielectric ( $\varepsilon_a$ ) and the diamagnetic ( $\chi_a$ ) anisotropies, (b) the three elastic moduli.

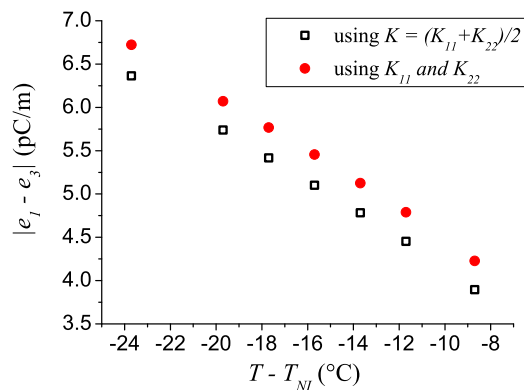


FIG. 12. (Color online) The temperature dependence of the combination  $|e_1 - e_3|$  of the flexoelectric coefficients.

higher than those by the first one; both values of  $|e_1 - e_3|$  fall in the regular range of that of rod-like nematics.

In order to check the consistency of our models and the obtained data, we have calculated  $U_{cFD}$  using the  $|e_1 - e_3|$  values determined from  $q_{cFD}$ . The results, depicted in Fig. 10b, show that the first model gave about 2% lower, while the second one about 11% higher values for  $U_{thFD}$  than the experiments.

Knowing the temperature dependence of  $|e_1 - e_3|$  gave us an opportunity to compare our results with the predictions of the molecular theory of flexoelectricity. It is expected [31–33] that the difference of flexoelectric coefficients should be proportional to the square of the order parameter  $S(T)$ :

$$|e_1 - e_3| = \hat{e}S^2(T), \quad (8)$$

where the proportionality constant is denoted by  $\hat{e}$ .

In Fig. 12  $|e_1 - e_3|$  is decreasing with the temperature, which is consistent with the similar tendency of



the order parameter. For a more quantitative comparison, the knowledge of  $S(T)$  would be essential.  $S(T)$  can only be accessed via measuring physical quantities that are directly coupled to it. The diamagnetic susceptibility, which is already determined from the Fredericksz-transition measurements (Fig. 11a) is a good candidate, since it should be proportional to  $S$  [35]:

$$\chi_a(T) = \hat{\chi}S(T), \quad (9)$$

where  $\hat{\chi}$  is a constant. In order to determine  $\hat{\chi}$ , and  $S(T)$ , the generalized form of the empirical Haller-extrapolation [34, 35] method is applied, via fitting the experimental data of  $\chi_a(T)$  with:

$$\chi_a(T) = \hat{\chi} \left(1 - \beta \frac{T}{T_{NI}}\right)^\gamma, \quad (10)$$

where  $\beta$ ,  $\gamma$  are constants, and the temperature data ( $T$ ,  $T_{NI}$ ) is measured in the Kelvin-scale. The result of the fit can be seen in Fig. 11a (solid line). The parameters of the best fit correspond to:  $\hat{\chi} = 1.64 \times 10^{-6}$ ,  $\beta = 1$ , and  $\gamma = 0.2$ . Besides the dimensionless SI quantity of  $\hat{\chi}$ , its molar version is often used:  $\hat{\chi}^M = \hat{\chi}M_m/\rho$ , where  $M_m$ , and  $\rho$  are the molar weight, and the density, respectively. Using  $M_m = 356.5 \frac{\text{g}}{\text{mol}}$ , and  $\rho = 1 \frac{\text{g}}{\text{cm}^3}$  one gets  $\hat{\chi}^M = 585 \times 10^{-6} \frac{\text{cm}^3}{\text{mol}}$ , that value fits well in the range of earlier results [35, 36] obtained for different compounds with two aromatic rings.

Combining Eq. (8) and Eq. (9) yields:

$$\chi_a = a\sqrt{|e_1 - e_3|}, \quad (11)$$

with  $a = \hat{\chi}/\sqrt{\hat{\epsilon}}$ .

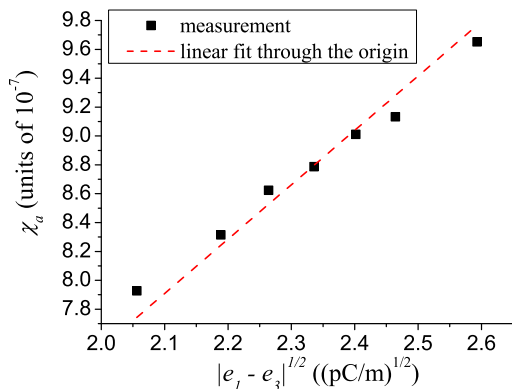


FIG. 13. (Color online) The relation between  $\chi_a$  and  $\sqrt{|e_1 - e_3|}$ .

Figure 13 provides a test of this relation, as it plots the measured  $\chi_a$  values against  $\sqrt{|e_1 - e_3|}$  calculated for the same temperatures (determined from the model with anisotropic elasticity). The fit corresponding to Eq. (11), represented by the dashed line, seems to be quite good in spite of the fact that there was only one fit parameter. The best fit results  $a = 0.38(C/m)^{-0.5}$ , that with  $\hat{\chi}$  determined above, yields  $\hat{\epsilon} = 18.6 \text{ pC/m}$ .

## IV. CONCLUSIONS

We have investigated the pattern forming phenomena induced by ultralow frequency sinusoidal voltages applied onto the calamitic nematic liquid crystal 1008. It was found that the behaviour in this low frequency range is characteristically different from that typical for high frequencies: here patterns appear as flashes in a short time interval within each half period of driving. Two kinds of pattern morphologies were detected: electroconvection rolls and flexodomains. The types of patterns differ in their wave vector (EC rolls are oblique to, while FDs are parallel with the initial director); moreover their flashes occur subsequently with a time separation, though in the same (and each) half period of driving. These scenarios are similar to those reported recently [8, 9] for the nematic mixtures Phase 5 and Phase 4.

Electric current measurements carried out simultaneously to pattern recording indicated strongly nonlinear current responses: the time dependence of the current showed sharp peaks after each polarity reversal of the applied voltage. The current nonlinearity in 1008 was much more pronounced than in Phase 5. This behaviour is attributed to the ionic conductivity of the liquid crystal. The transient current may be due to the motion of ions during building up a Debye screening layer at the electrodes, while the (insulating) polyimide coating ensuring the planar alignment blocks the charge transfer through the electrodes.

We found that, interestingly, the time instant of the flashing EC patterns (the time of the EC contrast peak) and that of the electric current peak coincide. This coincidence holds for all voltages, frequencies and temperatures that we have tested. The shape of the current signal is not affected by the occurrence of EC significantly, indicating that it originates from the more robust ionic effects described above. This is also supported by the fact, that the current peaks could be observed below as well as above the EC threshold, and even in the isotropic phase. We think, that the current peak has a significant effect on the formation of EC, but not vice versa; the appearance of the EC flashes is synchronized to the current peaks. Recently we reported a comparison [9] between the measured and the theoretically calculated time instant of the EC flashes for Phase 5. It indicated that in the experiment at ultralow  $f$  EC occurred earlier within the half period than expected from the extended standard model of EC [6, 10]. We suggest that the phase locking of EC to the ionic current peaks might be the reason for this mismatch (the extended standard model does not consider ionic effects). We guess that an adequate extension of the theory to weak electrolytes could reveal this problem and additionally explain the role of the robust current peaks in the pattern formation; proving that, however, represents a great theoretical challenge for the future.

Studying the threshold characteristics of the patterns we found that the behaviour of EC and FD are essentially different. Flexodomains have a sharp threshold, i.e. the

pattern contrast increases suddenly for  $U > U_c$ . For EC this holds only at high  $f$ ; reducing the frequency the EC threshold becomes gradually less sharp (the contrast changes smoothly with the voltage). On the one hand it hinders the precise determination of the EC threshold. On the other hand, we showed that this tendency can be followed quantitatively using an imperfect bifurcation model. In this approach the amount of imperfection increases as the frequency is lowered.

EC and FD have different frequency dependence of their thresholds. At high  $f$  the EC threshold is lower, while at DC driving flexodomains are seen. Therefore it is not surprising that there is a crossover between EC and FD at around 60 mHz, where their thresholds become equal. Such a scenario was already anticipated from measurements on Phase 5, but could first be demonstrated explicitly now on 1008.

Interestingly, the two kinds of patterns can appear in the same half period in some frequency range on both sides of the crossover point, including frequencies where the two thresholds are quite different. This is made possible by the narrow time interval and time separation of the flashes.

The  $q_{cEC}(f)$  curve of 1008 shows a discontinuity at  $f_c \approx 7$  Hz, indicating a crossover from conductive to dielectric convection rolls. Interestingly, unlike similar crossovers reported at high frequencies in other compounds, here both the conductive and the dielectric rolls are oblique around this crossover frequency; consequently the Lifshitz-frequency is located in the dielectric regime. Though oblique dielectric rolls have already been reported recently in Phase 4 (which had no conductive regime at all) [8], to our knowledge 1008 is the first substance which exhibits the transition from oblique conductive to oblique dielectric rolls with increasing the frequency of the ac voltage. The low  $f_c$  indicates a fairly

low electrical conductivity which also helps distinguish between EC and FD patterns by increasing their time separation and may also be responsible for the enhanced nonlinearity of the current.

Measuring the critical wave number of the flexoelectric domains offers a way to calculate the combination  $|e_1 - e_3|$  of the flexoelectric coefficients using theoretical models based either on the one-elastic-constant approximation or on a rigorous handling of anisotropic elasticity. It has turned out that the values determined by the two methods differ only by about 7%. The reason for this small difference is that the relevant material parameters ( $K_{11}$ ,  $K_{22}$  and  $\varepsilon_a$ ) of 1008 fall into that range, where  $q_{cFD}$  is only slightly sensitive to the elastic anisotropy. The threshold voltages of FDs, calculated from the theoretical models using the above values of  $|e_1 - e_3|$ , show a satisfactory agreement with the measured data; this proves the consistency of the models.

In cooling 1008 has a nematic temperature range of about 25 degrees. The temperature dependence of the elastic moduli, the dielectric and the magnetic anisotropies was determined for the whole nematic range. For  $|e_1 - e_3|$  data could be obtained only for the lower temperature part of the nematic phase as flexodomains did not exist for  $T - T_{NI} > -8$  °C. The temperature dependence of  $|e_1 - e_3|$  was compared with that of  $\chi_a$ ; the latter being proportional to  $S(T)$ . It was found that  $|e_1 - e_3| \propto S^2$  is satisfied, as it is expected from the molecular theory of dipolar flexoelectricity, and also the proportionality constant was determined.

## ACKNOWLEDGEMENTS

Financial support by the Hungarian Research Fund OTKA K81250 is gratefully acknowledged. We also thank Werner Pesch for fruitful discussions.

- 
- [1] L. M. Blinov and V. G. Chigrinov, *Electrooptic Effects in Liquid Crystal Materials*, Springer, New York (1996).
  - [2] Yu. P. Bobylev and S. A. Pikin, *Sov. Phys. JETP*, **45**, 195–198 (1977).
  - [3] Á. Buka, N. Éber, W. Pesch and L. Kramer, In *Self Assembly, Pattern Formation and Growth Phenomena in Nano-Systems*, Eds. A. A. Golovin and A. A. Nepomnyashchy, Springer, Dordrecht, pp. 55–82 (2006).
  - [4] Á. Buka, N. Éber, W. Pesch and L. Kramer, *Physics Reports*, **448**, 115–132 (2007).
  - [5] E. Bodenschatz, W. Zimmermann and L. Kramer, *J. Phys. (France)*, **49**, 1875–1899 (1988).
  - [6] A. Krekhov, W. Pesch, N. Éber, T. Tóth-Katona and Á. Buka, *Phys. Rev. E*, **77**, 021705 (2008).
  - [7] M. Treiber and L. Kramer, *Mol. Cryst. Liq. Cryst.*, **261**, 311–326 (1995).
  - [8] M. May, W. Schöpf, I. Rehberg, A. Krekhov and Á. Buka, *Phys. Rev. E*, **78**, 046215 (2008).
  - [9] N. Éber, L. O. Palomares, P. Salamon, A. Krekhov and Á. Buka, *Phys. Rev. E*, **86**, 021702 (2012).
  - [10] A. Krekhov, W. Pesch and Á. Buka, *Phys. Rev. E*, **83**, 051706 (2011).
  - [11] L. Kramer and W. Pesch, In *Pattern Formation in Liquid Crystals*, Eds. Á. Buka and L. Kramer, Springer, New York, pp. 221–256 (1996).
  - [12] L. Kramer and W. Pesch, In *Physical Properties of Nematic Liquid Crystals*, Eds. D. A. Dummur, A. Fukuda and G. R. Luckhurst, Inspec, London, pp. 441454 (2001).
  - [13] E. Kochowska, S. Németh, G. Pelzl and Á. Buka, *Phys. Rev. E*, **70**, 011711 (2004).
  - [14] Á. Buka, T. Tóth-Katona, N. Éber, A. Krekhov and W. Pesch, In *Flexoelectricity in Liquid Crystals. Theory, Experiments and Applications*, Eds. Á. Buka and N. Éber, Imperial College Press, London, pp. 101135 (2012).
  - [15] M. Majumdar, P. Salamon, A. Jákli, J. T. Gleeson and S. Sprunt, *Phys. Rev. E*, **83**, 031701 (2011).

- [16] G. G. Nair, C. A. Bailey, S. Taushanoff, K. Fodor-Csorba, A. Vajda, Z. Varga, A. Bóta and A. Jákli, *Adv. Mater.*, **20**, 3138 (2008).
- [17] S. Rasenat, G. Hartung, B. L. Winkler and I. Rehberg, *Exp. Fluid*, **7**, 412 (1989).
- [18] G. Derfel, *J. Mol. Liq.*, **144**, 59–64 (2009).
- [19] F. C. M. Freire, G. Barbero, and M. Scalerandi *Phys. Rev. E*, **73**, 051202 (2006).
- [20] F. C. Freire, A. L. Alexe-Ionescu, M. Scalerandi, and G. Barbero *Appl. Phys. Lett.*, **89**, 214101 (2006).
- [21] G. Barbero, A. M. Figueiredo Neto, F. C. M. Freire, and J. Le Digabel *Phys. Rev. E*, **74**, 052701 (2006).
- [22] G. Barbero, G. Cipparrone, O. G. Martins, P. Pagliusi, and A. M. Figueiredo Neto *Appl. Phys. Lett.*, **89**, 132901 (2006).
- [23] A. L. Alexe-Ionescu, G. Barbero, and I. Lelidis *Phys. Rev. E*, **80**, 061203 (2009).
- [24] L.O. Palomares, J.A. Reyes, and G. Barbero *Phys. Lett. A*, **333**, 157-163 (2004).
- [25] R. Atasei, A.L. Alexe-Ionescu, J.C. Dias, L.R. Evangelista, and G. Barbero *Chem. Phys. Lett.*, **461**, 164169 (2008).
- [26] G. Barbero, F. Batalioto, and A. M. Figueiredo Neto *Appl. Phys. Lett.*, **92**, 172908 (2008).
- [27] S. P. Trainoff and D. S. Cannell, *Phys. Fluids*, **14**, 1340–1363 (2002) and references therein.
- [28] W. Pesch, private communication.
- [29] A. Hertrich, A.P. Krekhov, and W. Pesch *J. Phys. II (France)*, **5**(5), 733–743 (1995).
- [30] T. Tóth-Katona, N. Éber, Á. Buka and A. Krekhov, *Phys. Rev. E*, **78**(3), 036306/1-12 (2008).
- [31] W. Helfrich, *Z. Naturforsch.*, **26a**, 833-835 (1971).
- [32] A. Derzhanski and A. G. Petrov, *Phys. Lett.*, **36A**(6), 483-484 (1971).
- [33] M. A. Osipov, In *Flexoelectricity in Liquid Crystals. Theory, Experiments and Applications*, Eds. Á. Buka and N. Éber, Imperial College Press, London, pp. 932 (2012).
- [34] F. Leenhouts, W. H. de Jeu and A. J. Dekker, *J. Phys. (France)*, **40**(10), 989–995 (1979).
- [35] R. Stannarius, In *Handbook of Liquid Crystals*, Eds. D. Demus, J. Goodby, G. W. Gray, H. W. Spiess, V. Vill, Wiley-VCH, Weinheim, Vol. 2A, pp. 113–127 (1998).
- [36] I. H. Ibrahim and W. Haase, *J. Phys. (France) Coll.*, **40**(C3), 164–168 (1979).